10th CIGRE Southern Africa
Regional Conference
2nd – 4th November 2021
Johannesburg, South Africa

# A 12 Month Field Trial of Novel Conductor Coatings for Increased Ampacity: Performance and Durability

**Dr Oliver Higbee[1], Dr Niall Coogan[1], Dr Andrew Swanson[2]**
**AssetCool[1]**
**The University of Kwazulu-Natal[2]**

## SUMMARY

Overhead conductors are limited in their current carrying capacity by the Maximum Allowable Conductor Temperature (MACT). Overhead conductors which operate at lower temperatures for a given cross sectional area and current are desired. This will increase the current carrying capacity for a cross sectional area and reduce power losses at a specified ampacity. Radiative cooling of overhead conductors via a Spectrally Selective Coating (SSC) represents an opportunity to achieve this. SSCs work by the simultaneous reflection of solar radiation (solar reflectance above 0.8) and increase in surface emissivity (emissivity above 0.9). A multi-strand research project was conducted at The University of Kwazulu-Natal, Durban, South Africa to test SSC conductors. Performance and durability were assessed with a field trial of SSC coated (test) conductors in comparison to control (uncoated) conductors for 16 months. Additional research on stability to high electric fields, and mechanical stability to aeolian vibrations is presented. The coating was demonstrated to cool conductors by up to 24%. Regarding durability, the coatings demonstrated a 0.05% performance drop off after 12 months of field operation as well as stability to the other accelerated testing.

## KEYWORDS

Overhead Conductor, Ampacity, Coating, Power Losses

## 1 INTRODUCTION

A critical component of the transmission and distribution (T+D) system with respect to performance and efficiency is the thermal rating of overhead conductors. Higher conductor temperatures result in a lower current carrying capacity and increased T+D losses [1]. High levels of solar radiation coupled with persistently high ambient temperatures result in higher conductor temperatures, reduced current carrying capacity and increased transmission losses [2]. Exceeding the Maximum Allowable Conductor Temperature (MACT) is a risk as conductor temperature is a variable which varies in time and space along the spans [3]. Thermal stress occurs when the MACT is exceeded. This results in lower sag vertical clearance, tensile loss, elongation and creep, and reduced life span of the conductors [4], [5]. This can result in conductor failure and expensive remediation works [6]. Solutions to reduce conductor temperature during operation are required, as this will increase ampacity or reduce power losses.

The heat balance equation which determines conductor temperature [7] outlines two primary heat transfer mechanisms: convection (cooling by the wind) and radiative cooling (heat dissipation by radiative heat transfer in the infrared spectrum). Using established technical brochure CIGRE 601 [8], for a conductor in equilibrium, its temperature is dependent on four main thermal mechanics given by Equation 1.

Corresponding author: niall.coogan@assetcool.com

$$P_J + P_S = P_C + P_R \quad (1)$$

Where; $P_J$ and $P_S$ are joule and solar heating and $P_C$ and $P_R$ are convective and radiative cooling. To decrease the conductor temperature, the heating terms need to be minimised and the cooling maximised. This paper provides research on the extent to which engineering the surface characteristics for optimal radiative cooling can improve the capacity and efficiency of overhead T+D conductors. A Spectrally Selective Coating (SSC) was formulated especially for application to overhead conductors in order to minimise solar absorption and maximise thermal emissivity. SSC coated conductors were tested in an ongoing (16 months to date) field trial against uncoated conductors to provide insight into the performance benefits and durability of coated conductors in the field. In addition to this, extra data is provided from long term medium voltage exposure outdoors, as well as mechanical stability to vibrational forces according to IEC 62568 - Overhead lines - Methods for fatigue testing of conductors.

## 2 THEORY

### 2.1 Photonics

Solar and infrared radiation (IR) have the potential to impact conductor ampacity. These two regions of the electromagnetic spectrum occur at different wavelengths. The solar radiation spectrum exists between 0.4µm and 2.5µm comprising of UV, visible light and near infrared light. IR radiation exists up to 1000µm, but the wavelengths of interest with respect to surfaces are 2.5µm - 25µm. When radiation interacts with a body it may be reflected (R), transmitted (T) or absorbed (A). These three phenomena are linked in the conservation of energy by: A + R + T = 1. From [8] we know radiative cooling and solar heating are given by Equations 2 and 3.

$$P_r = \pi D \varepsilon_S \sigma_B [(T_S + 273)^4 - (T_A + 273)^4] \quad (2)$$

Where: $P_r$ = radiation (heat) loss (W/m), $D$ = conductor diameter, $\varepsilon_S$ = emissivity coefficient of conductor surface, $\sigma_B$ = Stefan Boltzmann constant, $T_S$ and $T_A$ = conductor and ambient temperature respectively.

$$P_S = \alpha_S . D . I_S \quad (3)$$

Where: $P_S$ = solar heat gain (W/m), $\alpha_S$ = absorptivity of the surface of the conductor, $D$ = conductor diameter and $I_S$ = intensity of solar radiation.

In essence, to optimise a conductor's surface for radiative cooling, solar absorption (α) needs to be minimised and thermal emissivity (ε) need to be maximised. Figure 1 shows typical emissivity and absorptivity of different surfaces. As shown, the spectrally selective coating has a low solar absorptivity (0.1) and high IR emissivity (0.93); this is made possible by using a metamaterial, which can simultaneously have optimal photonic properties in both the solar and infrared parts of the spectrum. Typically a material is either emissive or reflective whereas in a metamaterial it can be both if they occur in different parts of the spectrum.

Corresponding author: niall.coogan@assetcool.com

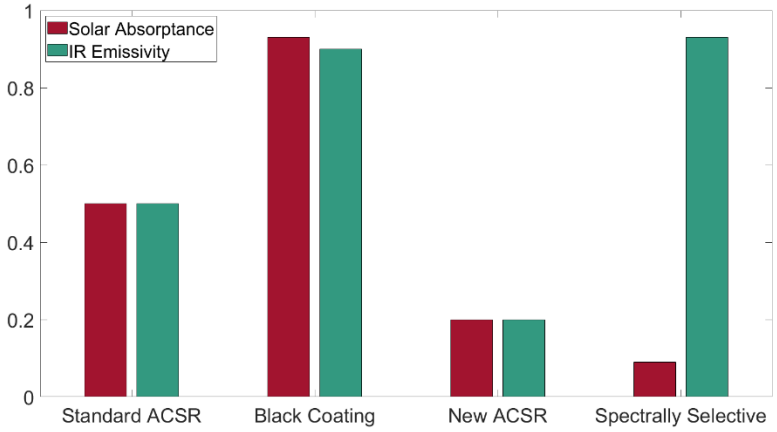


**Figure 1: The solar absorptance (red) and infrared emittance (green) of different surfaces. ACSRs are both inefficient at dissipating heat and reflecting the sun's energy. The spectrally selective coating reflects the sun's energy effectively and is highly emissive.**

### 2.2 CIGRE 601

α and ε are standard parameters in the CIGRE 601 calculator, therefore it is possible to calculate a theoretical ampacity increase using ratings guidance for the RSA climate taken from Eskom [9]. These calculations, reported in Table 1, suggest ampacity gains of 14.9% are feasible using the deterministic ratings parameters.

**Table 1: Comparison of SSC and uncoated conductor ampacity. Environmental conditions: 40°C, wind speed 0.5 m/s, wind direction 90° to the conductor axis, 1120 W/m² solar intensity.**

| | Uncoated Rabbit ACSR | SSC Rabbit ACSR | Improvement |
|---|---|---|---|
| Absorptivity, α | 0.5 | 0.1 | |
| Emissivity, ε | 0.5 | 0.93 | |
| Ampacity at 75°C MACT (A) | 199.0 | 228.6 | 14.9% (Ampacity increase) |
| Temperature at 228 A (°C) | 85.2 | 75.0 | 11.97% (Temperature Reduction) |

## 3 METHOD

### 3.1 Field Trial: Thermal Performance and Durability Testing

The experimental design for the thermal performance testing is as follows. 4 x 10m Rabbit ACSR conductors were sourced. Two were coated with a SSC designed to cool overhead conductors by increasing solar reflectivity and thermal emissivity. These were treated as the test conductors. The other Rabbit conductors were left as received and treated as control conductors. All conductors were connected electrically in series and high resolution conductor temperature data was measured from the core. A detailed explanation of the experimental set up is included in the appendix (8.1). This is a consistent experimental set up to previous research conducted by UK utilities, undertaken to improve the statistical ratings guidance for overhead lines [10]. Figure 2 shows images of the experimental set up. The field trial was started in March 2020, with weather and conductor data collected in one second intervals. Data collection was continuous outside of load shedding (periods of loss of power in the area).

Corresponding author: niall.coogan@assetcool.com

To test performance consistency, after 10 months of data collection, one of the coated conductors was replaced by a new coated conductor. This allowed for the side by side comparison of new vs aged conductors with 10 months field exposure for a quantitative comparison of performance consistency over time. The temperatures of the new and aged conductors were correlated via linear and rank correlation analysis to provide a range of correlation coefficients to compare the consistency of performance.

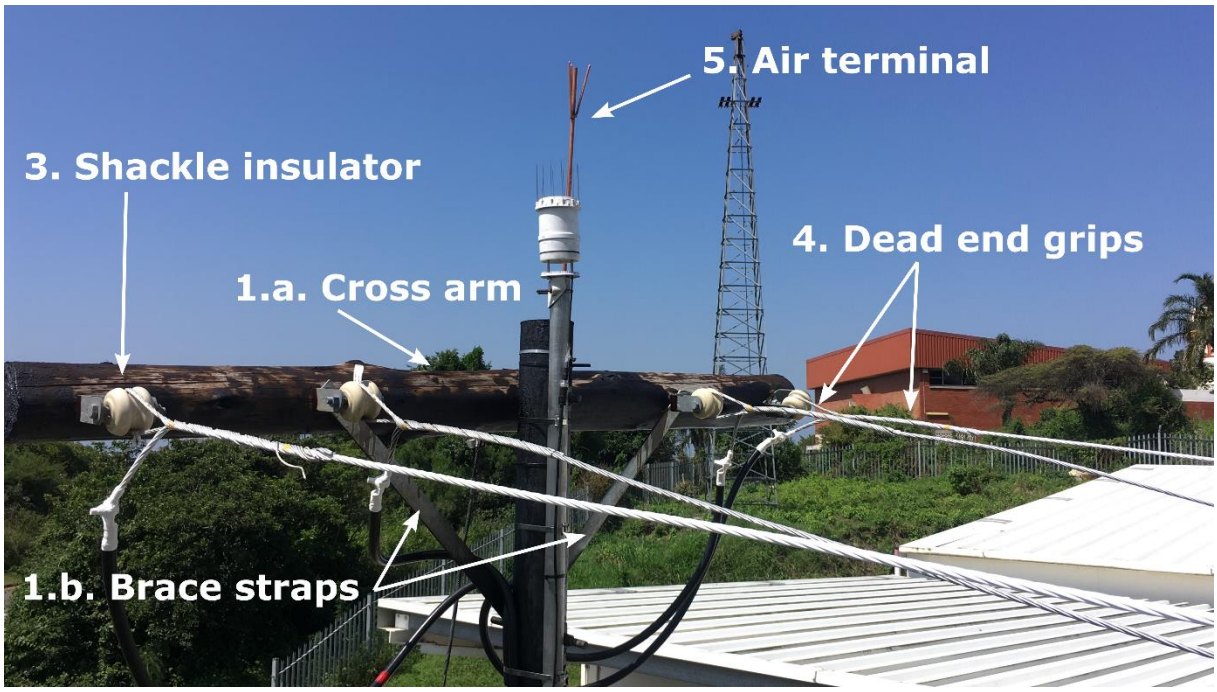


**Figure 2: Experimental set up at the cross arm**

It is noted that transmission assets have long asset life cycles (upwards of 30 years). It is important to demonstrate any tested material has the appropriate durability and stability under a wide variety of environmental stresses. Alongside the testing at UKZN, a wide range of accelerated laboratory testing was performed, including hardness, impact resistance, UV stability, corrosion stability, temperature stability, chemical stability, $SO_2$ resistance, moisture stability and humidity stability. These results will be published elsewhere as outlined in the 'Future Research Section'.

### 3.2 Medium Voltage Testing

As the thermal performance testing was conducted at low voltage DC, it is important to show material stability and resistance to environmental dirt accretion at higher voltages where the electric field has the potential to attract particulate dirt. A second rig was constructed to inspect this and 4 x 10m Rabbit ACSR conductors were sourced. Three were coated with a spectrally selective coating. These were treated as the test conductors. The fourth conductor was left as received and treated as the control conductor. The conductors were suspended at a height of 6.5m by distribution poles, spaced 10m apart. The line was insulated to 33kV and supplied by a dual phase 33kV transformer. The experimental setup is shown in Figure 3. This test offers a realistic insight into the performance of a conductor subject to an electric field strong enough to attract significant pollutants. By modelling the conductors as ideal cylinders, the electric field was calculated for each conductor in Table 2.

Corresponding author: niall.coogan@assetcool.com

**Table 2: Electric field strengths incident on the conductors**

| Line number | Electric field strength kV/cm |
|---|---|
| 1 | 3.5 |
| 2 | 4.5 |
| 3 | 4.1 |
| 4 | 3.0 |

To observe the SSC's ability to self-clean and remain stable under these electric fields, a visual inspection was untaken at various time intervals from 1 to 100 days, in the form of photographs.

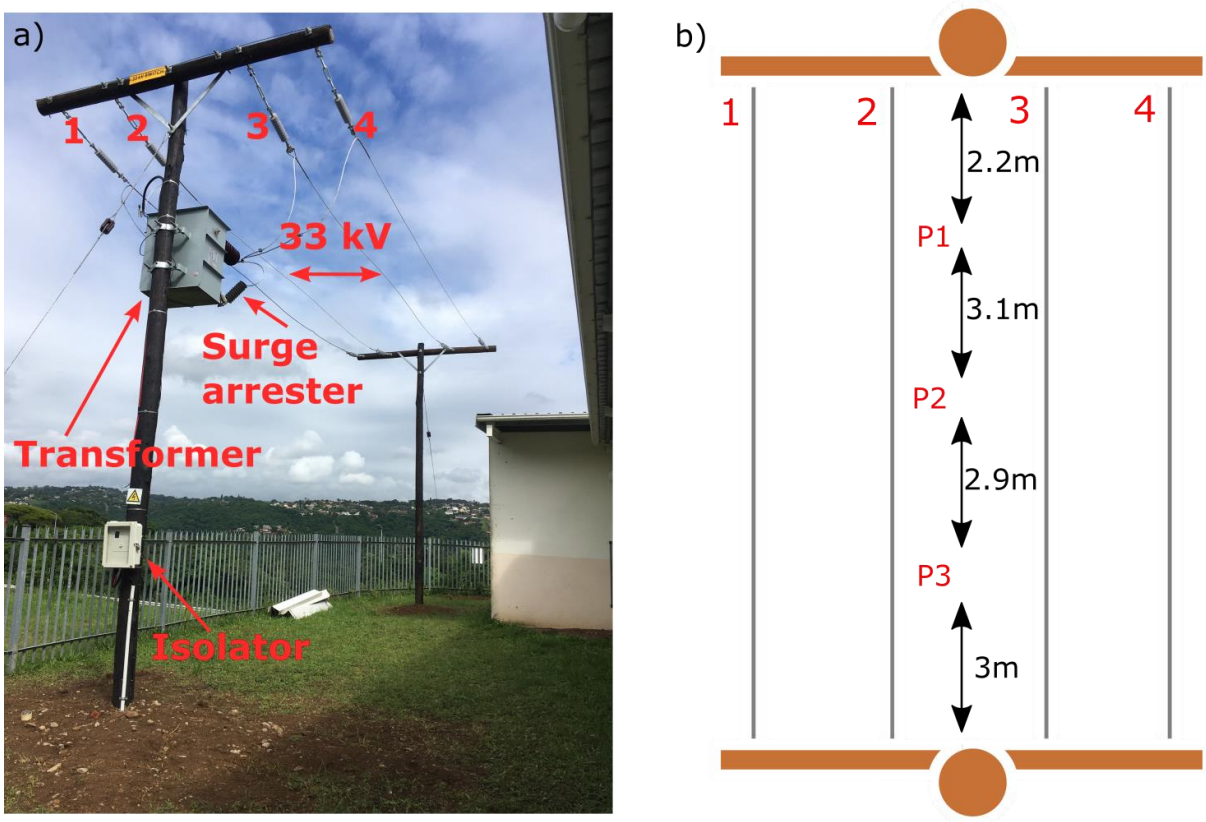


**Figure 3: a) Medium Voltage field trial setup. b) Position of photographs (P1, P2, P3) along conductors.**

### 3.3 Vibrational Testing

Aeolian vibrations occur as wind energy induces resonant standing waves on the conductor. The wavelength and frequency of the vibration is determined by the wind speed. Such vibrations have the potential to damage a material on the surface of conductors if insufficiently mechanically robust. The stability of the coating at resonant frequencies was tested following the guidelines in IEC 62568 - Overhead lines - Methods for fatigue testing of conductors [11]. A detailed experimental overview and images of the set up are included in the appendix (8.2). The experiment was adapted from previous vibrational conductor research [12]. The coated conductor was tested at resonant frequencies corresponding to wind speeds between 1 to 7m/s, in 1m/s intervals. Each test lasted 24 hours and the conductor was subjected to a total of 46 million cycles at various amplitudes. The conductor was inspected visually after the testing and photographs were taken.

Corresponding author: niall.coogan@assetcool.com

# 4 RESULTS

## 4.1 Field Trial: Thermal Performance and Durability Testing

### Descriptive Weather Statistics

Table 3 shows the average weather for each of the latest 6 months of the field trial. The results demonstrate high ambient temperatures and humidity, and consistent wind speeds, which allows for good comparisons between data collected in different months.

**Table 3: Descriptive weather statistics for months 11-16 of the field trial**

| Date | Month of trial | Ambient (°C) | Wind Speed (m/s) | Solar Intensity (W/m$^2$) | RH (%) |
|---|---|---|---|---|---|
| January 2021 | 11 | 23.9 | 1.8 | 99.8 | 84.3 |
| February 2021 | 12 | 23.9 | 1.8 | 91.0 | 83.1 |
| March 2021 | 13 | 23.2 | 1.6 | 79.3 | 82.5 |
| April 2021 | 14 | 22.0 | 1.6 | 74.5 | 80.4 |
| May 2021 | 15 | 21.0 | 1.6 | 94.9 | 72.8 |
| June 2021 | 16 | 19.7 | 1.9 | 116.9 | 69.8 |

### Conductor Temperatures

Conductor temperature data was collected from the thermocouples and first z-scored to remove anomalies [13]. Then means over 1 minute, 15 minutes, 24 hrs and a month were taken. Table 4 shows the average conductor temperature each month; periods of load shredding were removed from these datasets. The data presented was collected from the conductors installed at month 1 of the trial. The average cooling seen was between 9.6 and 13.1% in line with CIGRE 601 estimations.

**Table 4: Average monthly cooling for months 11-16 of the field trial**

| Date | Month of trial | Uncoated (°C) | SSC (°C) | Cooling (%) |
|---|---|---|---|---|
| January 2021 | 11 | 71.5 | 64.0 | 10.3 |
| February 2021 | 12 | 65.4 | 58.6 | 10.1 |
| March 2021 | 13 | 72.2 | 64.9 | 9.6 |
| April 2021 | 14 | 74.1 | 65.4 | 11.5 |
| May 2021 | 15 | 73.4 | 63.6 | 12.9 |
| June 2021 | 16 | 70.3 | 60.8 | 13.1 |

To investigate peak performance, the 1 minute interval data was explored. These peak differences occur in ‘worst case scenarios’: when the wind speed is low, ambient temperatures are high and solar intensity is high. In reality, these “worst case” conditions were rarely found, but periods of low wind speed were, which is the weather parameter which has the largest impact on conductor temperature. Peak cooling between 20.1% and 24.0% were found in each month, shown in Table 5. It can also be seen that the uncoated conductor was in excess of MACT in many of these peaks where the SSC was not; this is an indicator of the increased line rating the SSC can provide. This is more clearly shown in Figure 4.

Corresponding author: niall.coogan@assetcool.com

**Table 5: Peak cooling for months 11-16 of the field trial**

| Time Stamp | Month of trial | Uncoated (°C) | SCC (°C) | Cooling (%) |
|---|---|---|---|---|
| 23 January 22:55 | 11 | 121.0 | 94.7 | 21.8% |
| 28 Feb 02:15 | 12 | 100.2 | 80.1 | 20.1% |
| 03 March 04:00 | 13 | 102.9 | 78.8 | 23.5% |
| 23 April 12:05 | 14 | 70.4 | 53.9 | 23.4% |
| 25 May 18:42 | 15 | 110.2 | 83.8 | 24.0% |
| 22 June 08:25 | 16 | 96.5 | 74.2 | 23.1% |

Finally, another key advantage of the SSC is highlighted: energy savings. Using the differences in resistance caused by the difference in operating temperatures between the conductors, energy savings ($I^2R$) were calculated on peak cooling days and extrapolated to a kilometre span, shown in Table 6.

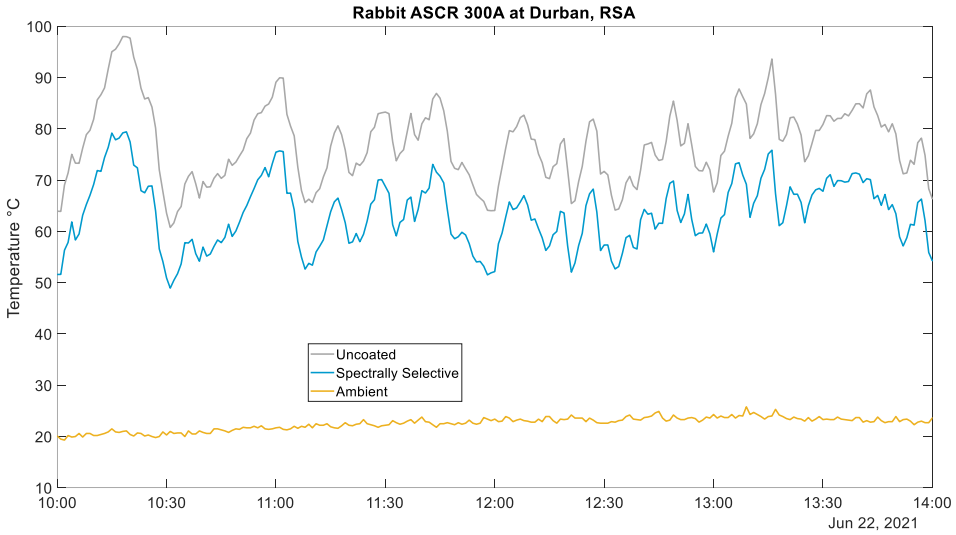


**Figure 4: Coated and uncoated Rabbit ASCR conductor temperatures in Durban, RSA at 300 A DC. Ambient air temperature shown in gold. Average metrological data. Wind speed = 1.14 m/s, direction = 98° solar radiation =216 W/m².**

**Table 6: Power loss reduction calculations based on lower temperatures**

| Time Stamp | Month of trial | Uncoated (°C) | Coated (°C) | Cooling (%) | Energy savings per km (kWh) | Reduction in energy losses (%) |
|---|---|---|---|---|---|---|
| 29 Jan | 11 | 84.1 | 74.7 | 10.8 | 44.8 | 3.0 |
| 04 Feb | 12 | 78.5 | 69.3 | 11.6 | 43.5 | 3.0 |
| 23 March | 13 | 81.0 | 71.2 | 12.0 | 46.5 | 3.2 |
| 11 April | 14 | 81.7 | 70.8 | 12.9 | 51.3 | 3.4 |
| 25 May | 15 | 88.4 | 73.7 | 16.3 | 69.5 | 4.6 |
| 13 June | 16 | 77.2 | 66.7 | 13.1 | 49.7 | 3.4 |

## Performance Consistency

Analysis of the new (installed at month 10) and aged (month 1) coated conductors was completed and Figure 5 and Table 7 show the temperature correlation between the coatings.

Corresponding author: niall.coogan@assetcool.com

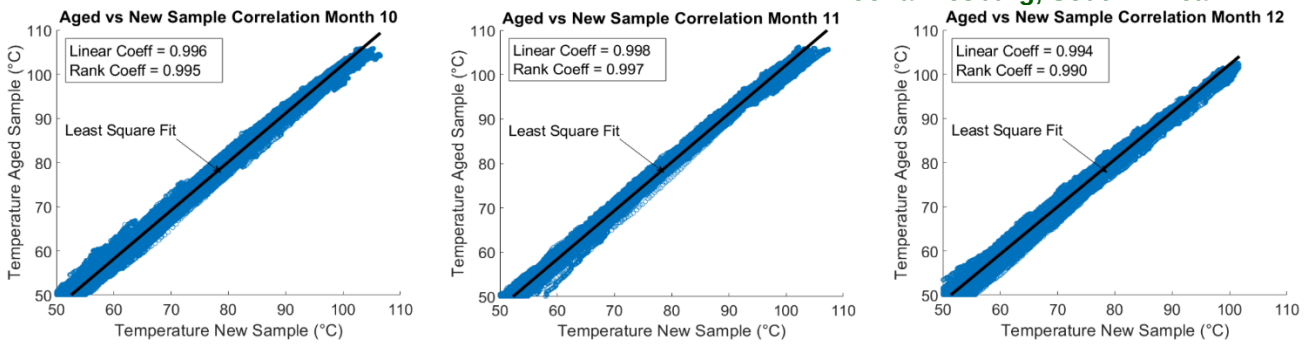


**Figure 5: Correlation plots for months 10/11/12 of the trial for the temperatures between the coated and uncoated samples.**

**Table 7: Correlation Coefficients for Performance Consistency Plots**

| Trial Month | 10 | 11 | 12 | Avergae |
|---|---|---|---|---|
| Linear Correlation Coeffcient | 0.996 | 0.998 | 0.994 | 0.996 |
| Rank Correlation Coeffcient | 0.995 | 0.997 | 0.990 | 0.994 |

The correlation plots demonstrate a 0.995 correlation coefficient demonstrating a performance drop off of less than 0.005, or a 0.5% drop off after 12 months.

### 4.2 Medium Voltage Stability

Photographs were taken at the same position for each inspection according to the position shown in Figure 3. Dirt particles temporarily adhered on the conductors after installation but were crucially seen to be removed from the coated conductors, validating the presence of active self-cleaning. Photographs from the first 100 days are shown in Figure 6. Comparison between photographs is complicated by the white balance differences in the photographs, where the conductor appears darker on days where the background is brighter. However initial results are promising, with no significant discolouration, cleaning of particles from the surface and no presence of flakes or deterioration.

**Figure 6: Photographs of Conductor 2 on Days 1, 60 and 94 (left to right)**

### 4.3 Vibrational Stability

After 46 million resonant oscillations, at frequencies corresponding to wind speeds between 1m/s and 7m/s, no indication of wear or deterioration was observed. Figure 7 shows the conductor after a 24 hr tests at a resonant frequency corresponding to 3m/s wind speed.

Corresponding author: niall.coogan@assetcool.com

**Figure 7: Photographs after a 24 hour vibrational test at 55Hz showing no detachment or damage.**

## 5 DISCUSSION, FUTURE WORK AND CONCLUSIONS

This paper presents the data on a multistrand research project testing the performance and durability of SSC conductors. Up to 24% cooling has been demonstrated with a 99.5% consistency over a 12 month period. This highlights the strong potential for cooling in addition to high levels of performance consistency. Critically, the coating at month 16 continues to demonstrate improved cooling of up to 23% in month 16. Outside of the cooling field trial, the coating was demonstrated to be highly resistant to electrical field induced dirt accretion through a dedicated long term MV outdoor field trial, with photo evidence of active dirt shedding to maintain solar reflectance throughout service. Beyond this, additional benefits have been demonstrated in corona noise reduction as well as strong mechanical stability to aeolian vibrations as simulated by IEC 62568.

Accordingly, this multi-strand research project will continue to present data on SSC conductors. Future work will involve the continued reporting of the field trial over time, presenting further data on in field durability and performance. Significant ongoing data collection on accelerated aging (UV/corrosion *etc.*) will be published in detail to show how accelerated lab tests correlate to in-field durability. We will further report on the alignment of empirical vs theoretical performance predictions of SSC conductors via a comparison of the empirical data collected in this field trial and that simulated by CIGRE 601.

## 6 BIBLIOGRAPHY

[1] H. Wan, J. D. McCalley, and V. Vittal, “Increasing thermal rating by risk analysis,” *IEEE Trans. Power Syst.*, vol. 14, no. 3, pp. 815–828, 1999.

[2] G. Liu, Y. Li, S. Liu, X. Dong, F. Qu, and Y. Li, “Real-time solar radiation intensity modeling for dynamic rating of overhead transmission lines,” in *2016 Australasian Universities Power Engineering Conference (AUPEC)*, 2016, pp. 1–6.

[3] M. Matus *et al.*, “Identification of critical spans for monitoring systems in dynamic thermal rating,” *IEEE Trans. Power Deliv.*, vol. 27, no. 2, pp. 1002–1009, 2012.

[4] N. M. Zainuddin *et al.*, “Review of Thermal Stress and Condition Monitoring Technologies for Overhead Transmission Lines: Issues and Challenges,” *IEEE Access*, vol. 8, pp. 120053–120081, 2020.

[5] J. Heckenbergerova, P. Musilek, and K. Filimonenkov, “Assessment of seasonal static thermal ratings of overhead transmission conductors,” in *2011 IEEE Power and Energy Society General Meeting*, 2011, pp. 1–8.

Corresponding author: niall.coogan@assetcool.com

[6] O. Armstrong, G. Southern, A. Carroll, and G. O'Brien, "Low wind speed occurrences and aging conductors: More than just a sag problem?," in *2018 IEEE/PES Transmission and Distribution Conference and Exposition (T&D)*, 2018, pp. 1–5.
[7] V. T. Morgan, "The thermal rating of overhead-line conductors Part I. The steady-state thermal model," *Electr. power Syst. Res.*, vol. 5, no. 2, pp. 119–139, 1982.
[8] T. B. Cigré, "601," *Guid. Therm. Rat. Calc. Overhead Lines, Work. Gr. B*, vol. 2, p. 43, 2014.
[9] Eskom, "DETERMINATION OF CONDUCTOR RATINGS IN ESKOM," 2015.
[10] M. Bertinat, R. Wood, and E. Marquand, "Improved Statistical Ratings For Distribution Overhead Lines (Phase 2) Final Report," 2018.
[11] IEC, "62568 - Overhead lines - Methods for fatigue testing of conductors," 2015.
[12] Y. D. Kubelwa, A. G. Swanson, and D. G. Dorrell, "Aeolian Vibrations of Overhead Transmission line Bundle Conductors During Indoor Testing, Part B: Assessment of Fatigue and Damping Performances," *CIGRE Sci. Eng. J.*, vol. 18, p. 96, 2020.
[13] P. J. Rousseeuw and M. Hubert, "Robust statistics for outlier detection," *Wiley Interdiscip. Rev. Data Min. Knowl. Discov.*, vol. 1, no. 1, pp. 73–79, 2011.

Corresponding author: niall.coogan@assetcool.com

# 7 APPENDIX

## 7.1 Field Trial Performance Set Up

The test and control conductors were suspended at a height of 5m from distribution poles, spaced 10m apart and connected electrically in series. The circuit was then connected to 3x1500w direct current (DC) power supplies able to supply up to 450A DC at up to 30V DC. Low volts DC current provides the necessary power to effectively study differences in current-temperature relationships between coated and uncoated samples. For this trial, the current was maintained at 300A. Eight T-type thermocouples were inserted into the conductor cores, and these were connected to a National Instruments CompactRIO chassis (cRIO-9040) *via* conditioned modules (2xNI-9213 Spring Terminal TC modules). Further, a dedicated weather station (ClimaVUE50) was installed on site to capture high resolution data, including air temperature, wind speed, wind direction and solar radiation, necessary inputs for the CIGRE 601 model [8].

When the power supplies were initiated, both lines experienced the same current as they are connected electrically in series. As the lines are spatially collocated and of the same orientation to the wind and the sun, we can assume environmental variables are constant across both conductors. Therefore, we can be confident that any difference in temperature is due to the surface properties of the conductor. Differential temperature-current profiles allow for the determination of additional current carrying capacity and added value to the network.

## 7.2 Vibrational Testing Experimental Plan

100m of Rabbit ACSR conductor was suspended and tensioned. A vibrational shaker was inserted 0.96m from the end. The measurement system consisted of National instruments cDAQ dataloggers connected to accelerometers, force transducers and a temperature log. The conductor was inspected for visible defects, spliced and pretensioned up to 30% of ultimate tensile strength (UTS) for 24 hours. The conductor was then re-tensioned to 20% of UTS (the typical design tension of Rabbit ACSR). The conductor was then inspected for visible defects where an image for every 1m of line was taken. Resonant vibrational frequencies (for a given wind speed) were estimated theoretically and then fine-tuned empirically to form resonant standing waves. The conductor was then vibrated at the set frequency and amplitude for a set duration. Data was recorded by the data logger for the test period. The conductor was then inspected for visible defects where an image for every 1m of line was taken. Images of the set up are shown in Figure 8.

Corresponding author: niall.coogan@assetcool.com

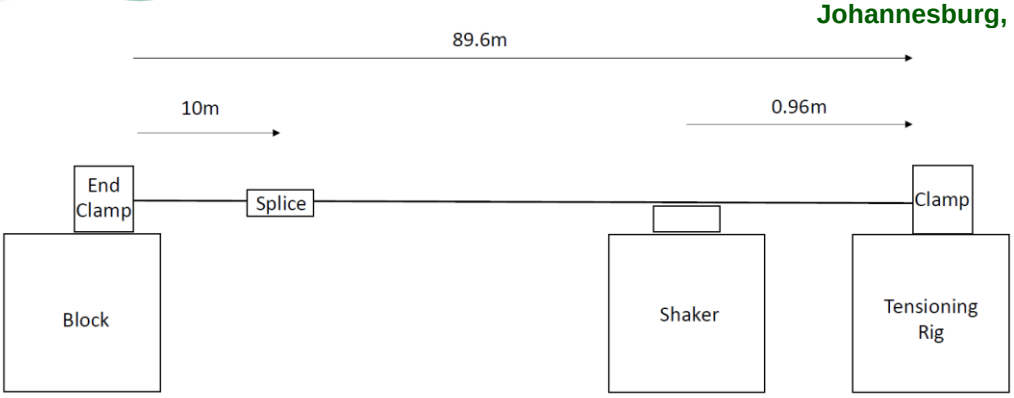



**Figure 8: Vibrational testing experimental set up**

Corresponding author: niall.coogan@assetcool.com